


## Article

# A Geochemical and Isotopic Investigation of Carbonatites from Huangshuian, Central China: Implications for Petrogenesis and Mantle Sources

Hao Zhao <sup>1,2,\*</sup>, Antonio Simonetti <sup>3</sup> , Stefanie Simonetti <sup>3</sup>, Xiaopeng Cao <sup>4</sup> and Yushan Du <sup>1</sup>

<sup>1</sup> Research Institute of Petroleum Exploration and Development, Shengli Oilfield Sinopec, Dongying 257015, China; duyushan817.slyt@sinopec.com

<sup>2</sup> Working Stations for Postdoctors of Shengli Oilfield, Dongying 257015, China

<sup>3</sup> Department of Civil and Environmental Engineering and Earth Sciences, University of Notre Dame, South Bend, IN 46556, USA; antonio.simonetti.3@nd.edu (A.S.); simonetti.4@nd.edu (S.S.)

<sup>4</sup> Xianhe Oil Production Plant of Sinopec Shengli Oilfield Company, Dongying 257068, China; caoxiaopeng.slyt@sinopec.com

\* Correspondence: zhaohao716.slyt@sinopec.com

**Abstract:** The exact geological processes involved in the formation of subduction zone-related carbonatites remain ambiguous, along with their implications for crustal/carbon recycling in carbonatite melt generation. This study provides new geochemical and stable (C, O) and radiogenic (Sr, Nd, Pb) isotope data for Huangshuian carbonatite, located within the Lesser Qinling Orogen, with the aim to decipher its complex petrogenetic history. The carbonatites display elevated CaO, low MgO and alkali contents, and significant enrichments of Pb, Mo, and HREEs compared to typical carbonatites. The  $\delta^{13}\text{C}_{\text{PDB}}$  (−4.6 to −4.9‰) and  $\delta^{18}\text{O}_{\text{SMOW}}$  (+6.6 to +7.8‰) values plot within the field of primary igneous carbonatites. The carbonatites are characterized by consistent radiogenic isotopic compositions [ $(^{87}\text{Sr}/^{86}\text{Sr})_i = 0.70599\text{--}0.70603$ ;  $\epsilon_{\text{Nd}} = -10.4$  to  $-12.8$ ;  $^{206}\text{Pb}/^{204}\text{Pb} = 16.24\text{--}17.74$ ]. These combined results suggest that the carbonatites represent late-stage differentiation products of a parental, mantle-derived carbonatite melt. Their corresponding Sr-Nd-Pb isotopic compositions support the hypothesis that the Lesser Qinling carbonatites originate from a heterogeneous upper mantle source involving an EMI-like mantle component coupled with minor assimilation of the basement rocks. The parental carbonatite melt was derived by the melting of carbonate-bearing subcontinental lithospheric mantle metasomatized as the result of Early Triassic subduction of the Mianlue Ocean.

**Keywords:** carbonatite; Lesser Qinling Orogen; Huangshuian; C-O-Sr-Nd-Pb isotope; mantle source



**Citation:** Zhao, H.; Simonetti, A.; Simonetti, S.; Cao, X.; Du, Y. A Geochemical and Isotopic Investigation of Carbonatites from Huangshuian, Central China: Implications for Petrogenesis and Mantle Sources. *Minerals* **2024**, *14*, 953. <https://doi.org/10.3390/min14090953>

Academic Editors: Alexander G. Sokol, Feng Huang, Liang Guo, Xiyao Li, Zhiwei Wang and Vinod O. Samuel

Received: 6 August 2024

Revised: 9 September 2024

Accepted: 16 September 2024

Published: 21 September 2024



**Copyright:** © 2024 by the authors. Licensee MDPI, Basel, Switzerland. This article is an open access article distributed under the terms and conditions of the Creative Commons Attribution (CC BY) license (<https://creativecommons.org/licenses/by/4.0/>).

## 1. Introduction

Carbonatites are considered unique mantle-derived igneous rocks [1–3], which consist of >50% carbonate minerals [4] and are most notably enriched in rare earth elements (REEs), and other incompatible trace elements, such as Sr and Ba. Carbonatitic melts are extremely mobile as their low viscosities facilitate their rapid ascent, transport, and emplacement [5–7]. Their low viscosity reduces the likelihood of host rock–melt interaction/contamination during their ascent through the subcontinental lithospheric mantle and overlying crust; consequently, carbonatitic melts can preserve their inherited primary radiogenic isotope compositions from their upper mantle sources [8]. Additionally, their elevated Sr (>>1000 ppm) and Nd (100 s of ppm) contents buffer their mantle-inherited radiogenic isotope signatures against crustal contamination processes [1,9]. Hence, these combined chemical and physical properties render carbonatites as insightful probes into deciphering the chemical nature, metasomatic history, temporal evolution, and carbon cycle of Earth’s upper mantle [1,10–14].

Carbonatites occur in different tectonic environments [4], but predominantly within anorogenic settings related to intracontinental rifts (e.g., East African Rift) [11,15], and rarely hosted within oceanic plates (e.g., Cape Verde Islands) [13,16] and orogenic domains (e.g., Qinglin) [3,17]. Moreover, there remains much debate as to whether carbonatitic melts are derived exclusively within the lithosphere [10], the subcontinental lithosphere [18–20], or asthenosphere (or deeper levels of the mantle) [1,21,22]. Bell and Simonetti [1] hypothesized a heterogeneous (mixed) mantle source for most carbonatites [23,24] based primarily on the critical stable (C, O) and radiogenic (Nd, Sr, and Pb) signatures of young (<200 Ma) carbonatites worldwide. In brief, carbonatite melts are derived from a heterogeneous mantle source that may involve HIMU (high- $\mu$ ;  $^{238}\text{U}/^{204}\text{Pb}$  ratio) [25], EM I (enriched mantle I) [26], and FOZO (FOcal ZOne) [26], and have been linked to a volatile-rich, asthenospheric/plume mantle interacting with overlying lithosphere.

The Lesser Qinling carbonatite occurrences within the Qinling orogenic belt are situated in central China (Figure 1). Subsequent to the recognition of carbonatite-related mineralization, multiple commodities have been exploited, including REE, Mo, Nb, and U ores [3,27–29]. Numerous previous studies have investigated the chronology, mineralization, petrological evolution, mantle source, and tectonic setting of the carbonatite complexes within the Lesser Qinling [3,17,27,28,30–33]. The timing of generation and ore mineralization associated with these carbonatites occurred between 197 Ma and 225 Ma [31,32,34–37]. Huang [31] and Cao [35] reported Re-Os ages for molybdenite from Huangshuian (HSA) carbonatite and their record ages of  $209.5 \pm 4.2$  Ma and  $208.4 \pm 3.6$  Ma. A new and similar LA-ICP-MS U-Th-Pb age of  $207 \pm 4$  Ma was obtained for bastnäsite from this deposit [36]. The Lesser Qinling carbonatites are unique and important mineral resources, and host economic deposits of molybdenite with total reserves of approximately  $80 \times 10^4$  t Mo metal [27,35,38,39]. These carbonatites are associated with quartz and are characterized by relatively flat REE patterns with enrichment in HREEs, which is a distinct feature compared to most carbonatites worldwide [3,17,28,40]. The enrichment in HREEs and Mo for these carbonatites is attributed to significant crystal fractionation involving calcite and non-silicate minerals (e.g., oxides and apatite) coupled with precipitation of a C-H-O supercritical fluid enriched in HREE, Mo, Si, and sulfate [17,32,33]. In an alternative hypothesis, the carbonatite magmas metasomatized the thickened eclogitic lower crust that produced high levels of Mo and HREE [3]. Moreover, the late-stage alteration with non-LREE-selective ligands (e.g.,  $\text{Cl}^-$ ,  $\text{CO}_3^{2-}$ ,  $\text{SO}_4^{2-}$ ) was suggested to account for the preferential HREE addition in the carbonatites [28].

Several previous investigations proposed that the Late Triassic Lesser Qinling carbonatites formed in a post-collisional extensional setting that occurred between the North and South China Blocks [30,33,41]. It is postulated that they are the result of fractional crystallization of primary alkaline silicate-carbonate melt derived from the partial melting of lithospheric mantle characterized by Sr-Nd-Pb isotopic compositions of EM I-like mantle [17,29–32]. Notably, it is postulated that their mantle sources contain recycled crustal materials [42] and are chemically enriched by subducted sedimentary carbonates [3,29]. Carbonate magmatism metasomatized the thickened eclogitic lower crust, which in turn may produce an enriched subcontinental lithospheric source [3,30]. Experimental petrology provides support for this latter hypothesis that involves the melting of carbonated eclogites at pressures  $> 2.5$  GPa [43,44]. Alternatively, Xu [45] argued that 15%–20% of lower crustal granulites were incorporated into the subcratonic mantle beneath the Qinling region. Çimen et al. [46] argue that the Miaoya carbonatite complex in South Qinling was derived from an isotopically heterogeneous mantle source containing recycled crustal carbon. Direct evidence for this interpretation is provided by the occurrence of a slab-derived eclogite xenolith identified within the Paleoproterozoic Fengzhen carbonatite in the North China craton [47].

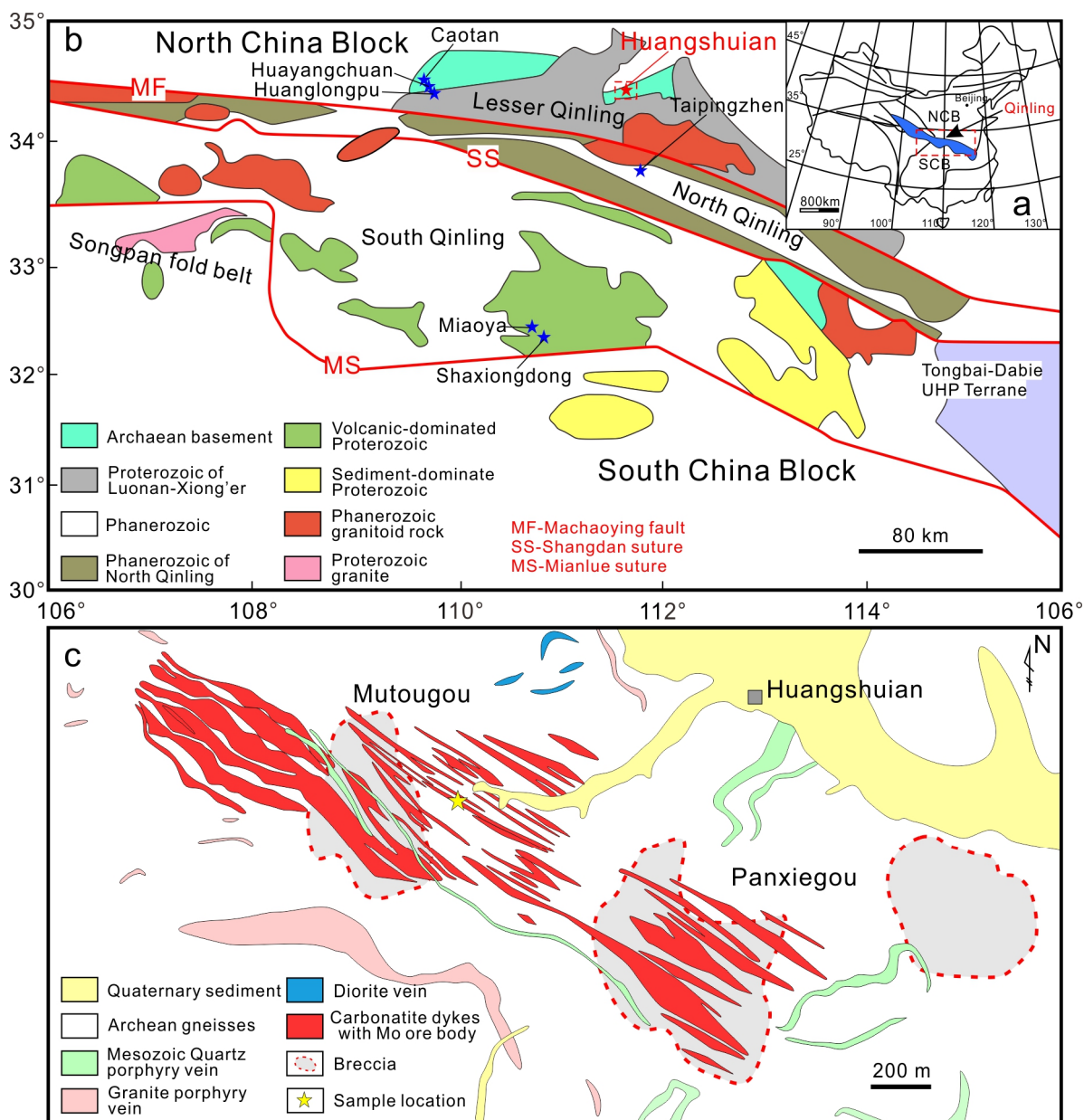


**Figure 1.** (a) Tectonic regions of China [30]. NCB—North China Block; SCB—South China Block. (b) Geological sketch map illustrating the locations of carbonatite complexes within the Qinling orogenic belt, including the HSA complex [30]. (c) Simplified geological maps of the HSA carbonatite complex [35].

To date, most previous investigations have focused on carbonatites located within anorogenic settings, whereas those related or found within collision/subduction zones have received relatively less attention [48]. In particular, there remains a lack of clear understanding of the geological processes involved, and systematic investigation of their genesis, source, and impact of crustal recycling on carbonatite melt generation. Thus, this study reports new stable (C, O) and radiogenic (Sr, Nd, Pb) isotope data, combined with major and trace elements signatures from the collision-related HSA carbonatite complex, in Lesser Qinling Orogen, central China (Figure 1). The geochemical and remaining isotope signatures will be used to decipher the complex petrogenetic history of the carbonatite and provide valuable insights into the chemical nature of its upper mantle source.

## 2. Geological Setting and Sample Descriptions

The Qinling orogenic belt, located in central China, separates the South China Block from the North China Block. It is regarded as a multistage orogenic belt recording the closure of the northernmost Paleo-Tethys Sea, the final continental collision between the North China Craton and Yangtze Craton [49]. It can be tectonically divided into four sections from north to south and delineated by main sutures, namely the Lesser Qinling orogenic belt, the North Qinling orogenic belt, the South Qinling orogenic belt, and the Songpan fold belt at the northern margin of the Yangtze Craton (Figure 1a,b) [49]. The Lesser Qinling orogenic belt lies within the Huaxiong Block, which forms part of the southern margin of the North China Block and comprises a crystalline basement, i.e., Mesoarchean Taihua Group of amphibolite-to-granulite facies suite and Neoproterozoic Dengfeng Group of granite–greenstone affinity [50]. The basement is unconformably overlain by the ~1780 Ma Mesoproterozoic intermediate to felsic volcanic rocks of the Xiong'er Group [51]. In turn, the Xiong'er Group volcanics are overlain by the Mesoproterozoic littoral clastic and carbonate rocks of the Guandaokou Group, the Neoproterozoic shallow marine clastic and carbonate rocks of the Luanchuan Group, and the Cambrian to Ordovician passive marginal sediments [52]. The Mesozoic magmatic intrusions are widely distributed within the Lesser Qinling region and were emplaced mainly at 220~190 and 160~110 Ma. The former stage is dominated by alkaline granites, which are inferred to form in a post-collisional extensional environment [53]. The latter stage is characterized by Late Jurassic–Early Cretaceous granites and porphyries, commonly associated with Mo mineralization [54,55].

The carbonatite complexes in Lesser Qinling Orogen include Caotan (CT), Huayangchuan (HYC), Huanglongpu (HLP), and Huangshuiian (HSA) from west to east (Figure 1b). Compared to the HLP carbonatite, which was discovered earlier, the HSA carbonatite complex also contains a similar, significant economic value. It is in Songxian county within the western Henan Province (Figure 1c). HSA carbonatite typically occurs as dykes or veins and intrudes into the Neoproterozoic Taihua Group gneiss, and these extend from <1 m to >1 km in length and follow a main NW-trending fault [31]. The carbonatite dykes and gneiss are locally crushed and occur as breccia, and silicification, feldspathization, sulfuration, and carbonatization are generally common at their contact margins. Of note, carbonatite is associated with Mo-(REE) mineralization with an estimated Mo reserve of  $19.86 \times 10^4$  t with an average grade of 0.082 wt. % [35]. Huang [31] and Bai [33] detail and summarize the geology, petrography, geochemistry, and mineralization of the carbonatites, and their relationship to the molybdenum deposits at HSA and HLP. These previous studies postulated that these rocks were derived from extensive fractional crystallization of a common carbonated silicate parental melt generated from an EM1-like mantle based on their REE patterns and radiogenic isotope compositions.

The Lesser Qinling carbonatite has a complex mineral paragenetic sequence that involves three mineralization stages for the carbonatite veins: 1—an early quartz K-feldspar stage; 2—a middle sulfide–REE mineral stage, and a 3—late sulfate–biotite stage [33]. The HSA carbonatites are generally dominated by calcite, quartz, and K-feldspar, which show extremely uneven mineral distribution in a single dyke (Figure 2). The calcite is pink or white in color, medium- or coarse-grained euhedral. The quartz and K-feldspar are coarse-grained anhedral and crystallized earlier than calcite (Figure 2j,k). The mineralized carbonatite veins commonly contain variable amounts of accessory mineral phases including pyrite, galena, molybdenite, barite, and celestite with minor REE minerals (monazite, bastnäsite, and parisite). Molybdenite is closely associated with REE minerals and usually disseminated within the calcite and quartz microfractures in the form of disseminated and veined (Figure 2l). Lastly, other accessory minerals include aegirine (Figure 2e,j), augite, and magnetite.



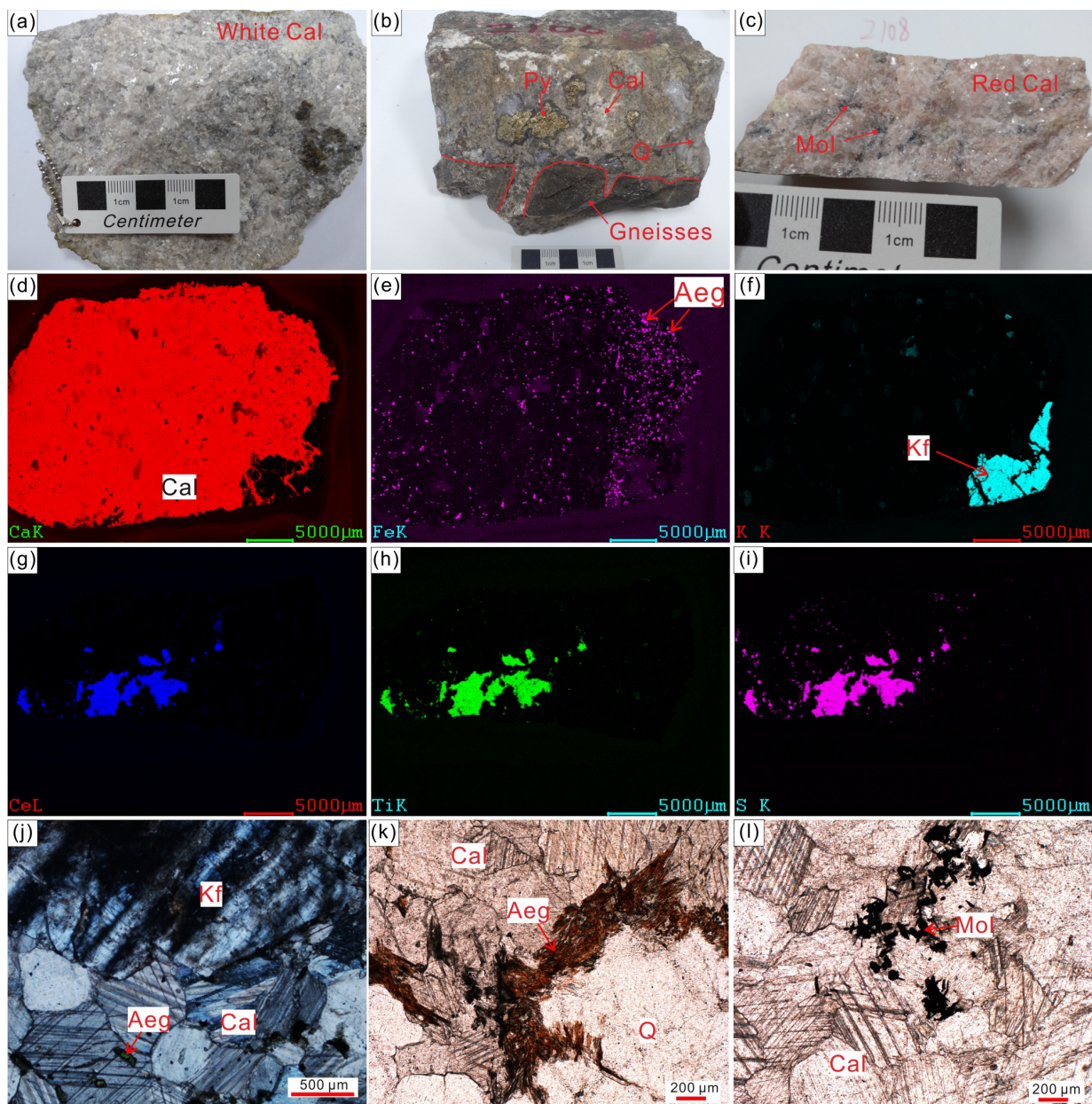


**Figure 2.** Photographs illustrating the textures and mineralogy of HSA carbonatite rocks investigated here. (a) Sample 2106 showing the white carbonatite with medium-grained calcite (Ca). (b) Sample 2106 exhibiting the contact margin between carbonatite and wall rock with silicification (Q: quartz) and sulfuration (Py: pyrite). (c) Sample 2108 representing pink carbonatite with sparsely disseminated molybdenite. Micro-XRF images illustrating distribution of Ca (d), Fe (e), and K (f) for sample 2104; Ce (g), Ti (h), and S (i) for sample 2108 showing the presence of calcite (Ca), fine-grained aegirine (Aeg), and K-feldspar (Kf). Photomicrographs for samples 2104 (j), 2105 (k), and 2108 (l) displaying the domination medium-grained calcite with early coarse-grained anhedral quartz and K-feldspar, and late interstitial aegirine and molybdenite (Mol).

### 3. Analytical Methods

Semi-quantitative major element compositional maps (Si, Al, Mg, Ca, Fe, Ti, K, P, S) for samples investigated here were produced with ~100  $\mu\text{m}$  thick petrographic sections using an Edax Orbis micro-XRF instrument (AMETEK, Inc., Berwyn, PA, USA) housed at the Center for Environmental Science and Technology (CEST), University of Notre Dame (UND). The chemical maps were generated using a 30  $\mu\text{m}$  beam overnight (~12 h) with

an amplification time of 12.8  $\mu$ s and a fluorescent energy of 32 kV. The major element concentrations for whole-rock sample powders were determined by ICP-OES (Inductively Coupled Plasma–Optical Emission Spectrometry, PerkinElmer, Inc., Waltham, MA, USA) within CEST (UND) using an external calibration technique, whereas trace element abundances were obtained by ICP-MS (Inductively Coupled Plasma–Mass Spectrometry) at the Midwest Isotope and Trace Element Research Analytical Center (MITERAC, UND). Trace element abundances were obtained using a Nu Plasma atom High-Resolution Inductively Coupled Plasma Mass Spectrometer (HR-ICP-MS, Nu Instruments Ltd., Wrexham, UK) in medium-resolution mode ( $M/\Delta M \approx 3000$ ) housed within MITERAC. At the start of each analytical session, the instrument was tuned and calibrated with a multi-element 1 ppb standard solution. The concentrations of the trace elements were determined by a standard/spike addition method [56], which includes corrections for matrix effects and instrumental drift.

The carbon and oxygen isotope analyses for calcite separates were conducted by reacting carbonate powder with concentrated  $H_3PO_4$  (100%) at 100 °C [57], using a Delta V Advantage isotope ratio mass spectrometer housed at CEST. Results are reported in per mil notation (‰) using standard delta notation relative to Peedee belemnite (PDB) and standard mean ocean water (SMOW). The accuracy of the  $\delta^{13}C$  and  $\delta^{18}O$  values reported here was validated by using three standards: NBS 19, YWCC, and ROYCC.

The bulk-rock Sr, Nd, and Pb isotope measurements reported here were analyzed using a NuPlasma II MC-ICP-MS instrument at MITERAC. Sr isotope measurements were determined using the protocols described in [58], with further details of ion exchange separation and collection for Sr outlined in [46]. Strontium isotope ratios were measured using 5 Faraday collectors in static, multi-collection mode and in dry plasma mode utilizing a DSN-100 desolating system (Nu Instruments, Wales, UK). The accuracy and reproducibility of the Sr isotope results were verified using a 100 ppb solution of the NIST SRM 987 strontium isotope standard, and the average value obtained for  $^{87}Sr/^{86}Sr$  ratio was  $0.710153 \pm 0.000027$  ( $2\sigma$  standard deviation;  $n = 6$ ); the Sr isotope ratios for the samples were therefore normalized to the accepted value for the NIST SRM 987 standard ( $^{87}Sr/^{86}Sr = 0.710245$ ). The Nd isotope ratios were determined using the same MC-ICP-MS instrument and following the analytical protocol described in [46]. REEs and Nd were sequentially separated using ion exchange columns containing AG50W-X8 and Eichrom Ln-Spec resins, respectively. The mass bias and drift for the instrument were calibrated using the repeated analysis of a 100 ppb solution of the JNdi-1 standard, which yielded an average  $^{143}Nd/^{144}Nd$  value of  $0.512090 \pm 0.000010$  ( $2\sigma$  standard deviation;  $n = 4$ ); the accepted  $^{143}Nd/^{144}Nd$  is 0.512115 [59].

The procedure for analyzing Pb isotope compositions via solution-mode MC-ICP-MS is described in [60]. The chemical separation and purification procedure involving ion exchange chromatography followed the procedures described by [61]. The purified Pb aliquot is spiked with a NIST SRM 997 Thallium standard solution (2.5 ppb) prior to analysis in dry plasma mode for instrumental mass bias correction based on the measured  $^{205}Tl/^{203}Tl$  ( $=2.3871$ ) for the NIST SRM 997 Tl isotope standard using the exponential fractionation law. Prior to sample introduction, a baseline (“on-peak-zero”) measurement consisting of the gas and acid blank was conducted for 30 s. Throughout the two analytical sessions, a 25 ppb solution of the standard NIST SRM 981 Pb (spiked with 6 ppb NIST SRM 997 Tl standard) was also analyzed periodically. Repeated measurements ( $n = 9$ ) of the NIST SRM 981 + Tl standard solution yielded average values and associated ( $2\sigma$ ) standard deviations as follows:  $^{206}Pb/^{204}Pb = 16.936 \pm 0.021$ ,  $^{207}Pb/^{204}Pb = 15.491 \pm 0.009$ ,  $^{208}Pb/^{204}Pb = 36.697 \pm 0.009$ , which are within analytical uncertainty of the accepted values for this standard given the associated uncertainties [62].

### 4. Results

#### 4.1. Whole-Rock Geochemistry

The major and trace element results for HSA carbonatite samples investigated here are listed in Table S1 and trace element abundances illustrated in Figure 3. All carbonatite samples define low MgO and alkali abundances, and high and variable CaO (41.48–51.04 wt. %) contents, which are typical for calcicarbonatite [4] with CaO/(CaO + MgO + FeO + MnO) ratios of 96.0–96.8. The trace element signatures for HSA carbonatite reported here are similar in general, and completely overlap those previously reported for Lesser Qinling carbonatite except for the abundances of Mo (4.38–950 ppm), which are significantly higher than the average calcite carbonatite value of 12 ppm (Figure 3) [33]. The HSA carbonatite samples exhibit relatively consistent primitive mantle-normalized trace element patterns (Figure 3a), and are characterized by the enrichment of Ba, U, Pb, and Sr and strong depletion of the high-field-strength elements (HFSEs: Nb, Ta, Zr and Hf). They also display lower Rb and higher Pb and Y abundances relative to those for typical calcicarbonatite [4]. Of particular interest is the fact that these samples contain substantially higher HREE abundances compared to average carbonatite worldwide ([63] and references therein). The total REE abundances range from 895 to 4760 ppm for the HAS carbonatite samples, and chondrite normalized REE patterns display negative slopes with variable (La/Yb)<sub>N</sub> ratios that range from 9.28 to 62.16, and lack Eu anomalies (Figure 3b).

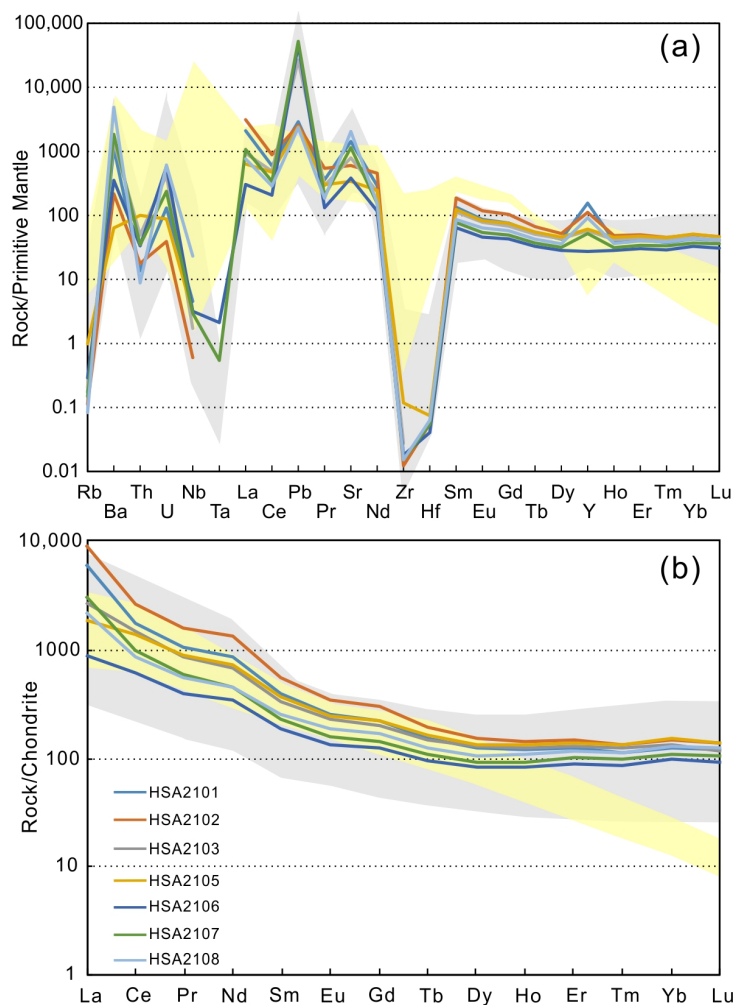


**Figure 3.** (a) Primitive mantle-normalized trace element spidergrams. (b) Chondrite-normalized REE patterns for samples of HSA carbonatite. Primitive mantle values and chondrite values are from [64]. The gray field represents the chondrite-normalized REE data for bulk carbonatites from Lesser Qinling [33], whereas the light yellow field represents compositions for average calcicarbonatite [4].



#### 4.2. C and O Isotope Compositions

The C and O isotope data obtained here for calcite separates from samples of HSA carbonatite and are summarized in Table S2 and illustrated in Figure 4. A majority of the calcite separates from carbonatite within the HSA complex record a remarkably uniform range of  $\delta^{13}\text{C}_{\text{PDB}}$  ( $-4.6$  to  $-4.9\text{‰}$ ) and  $\delta^{18}\text{O}_{\text{SMOW}}$  ( $+6.6$  to  $+7.8\text{‰}$ ) values, respectively, and plot within the field defined for “primary igneous carbonatites” (PIC). In addition, one sample (HSA2106) exhibits lower  $\delta^{13}\text{C}_{\text{PDB}}$  ( $-5.1\text{‰}$ ) but significantly lower  $\delta^{18}\text{O}_{\text{SMOW}}$  ( $+5.1\text{‰}$ ) values (Figure 4), and plots slightly to the left of the PIC box (Figure 4). The carbonate investigated here from HSA carbonatite displays similar C and O isotope compositions compared to those reported in [31,33], but has higher  $\delta^{13}\text{C}_{\text{PDB}}$  values relative to those recorded for carbonatite from the HLP complex [27,65].

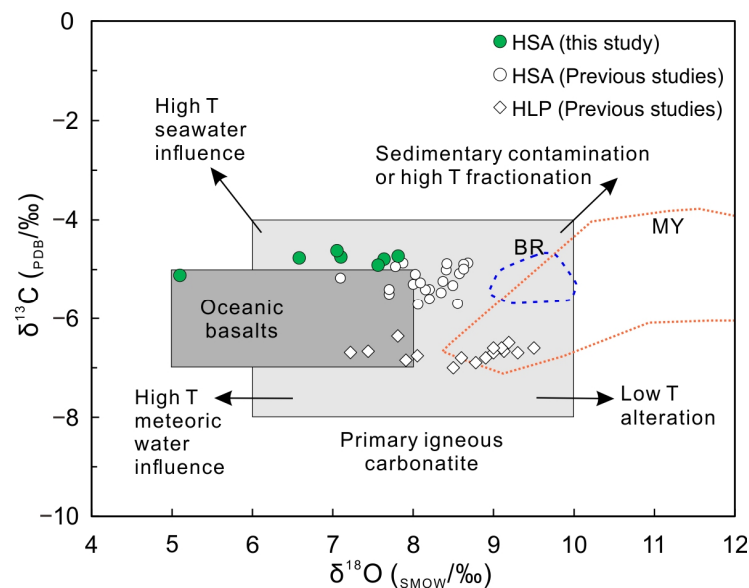


**Figure 4.** Illustrates carbon and oxygen isotopic compositions for carbonate separated from the HSA carbonatite samples investigated here. The white-colored points represent analyses for samples from HSA reported previously by [31,33]. These are compared to those carbonatites from HLP [27,65], South Qinling (MY) [45,46] and Blue River, Canada (BR) [66]. Primary igneous carbonatite field and oceanic basalts box as defined by [67]. Illustrated are the major processes responsible for changes in C–O isotopic composition of carbonatites [68].

#### 4.3. Sr, Nd, and Pb Isotope Compositions

The new Sr, Nd, and Pb isotopic data for samples of HSA carbonatite are listed in Tables S3 and S4 and displayed in Figures 5 and 6. The age of 208 Ma (molybdenite Re–Os) [35] for the HSA carbonatite has been adopted for the age corrections of measured isotope ratios.

The initial  $^{87}\text{Sr}/^{86}\text{Sr}$  isotope ratios for HSA carbonatites investigated here display a limited range with values between 0.70599 and 0.70603, which are slightly higher compared to the HLP carbonatites (Figure 5). The initial  $^{143}\text{Nd}/^{144}\text{Nd}$  ratios range between 0.51171 and 0.51184, which correspond to  $\epsilon_{\text{Nd}(t)}$  values of  $-10.4$  to  $-12.8$ , similar to the range of values previously reported for HSA carbonatites [31], and lower than those for HLP carbonatites [30]. The  $T_{\text{DM}}$  Nd model ages for the carbonatites range from 1.38 to 1.80 Ga (Table S3). The initial Sr isotope ratios are relatively close to the values expected for melts derived from an EM I (enriched mantle I) mantle component, but are more radiogenic in nature (i.e., higher Sr and lower Nd ratios).



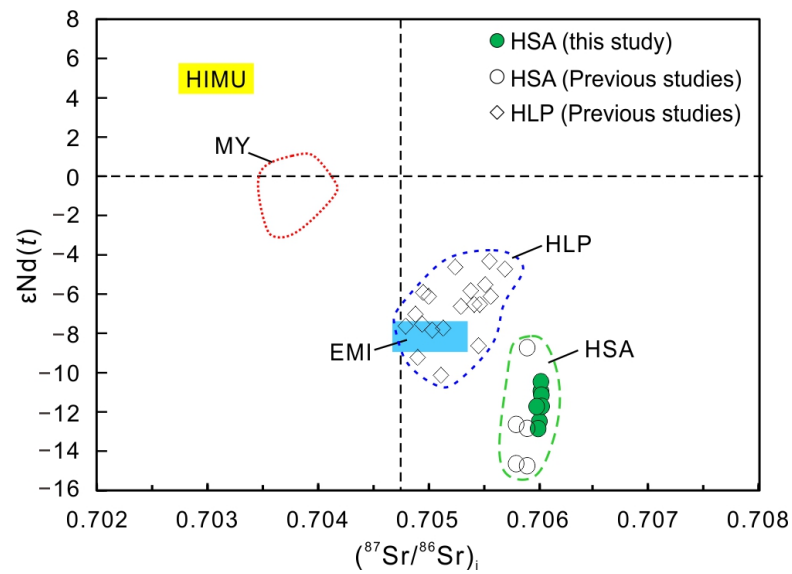


**Figure 5.** Diagrams of initial  $^{87}\text{Sr}/^{86}\text{Sr}$  vs.  $\epsilon_{\text{Nd}}(t)$  values for samples of HSA carbonatite. These are compared to initial Sr and Nd isotope data reported for those carbonatites from Lesser Qinling [30,31], and South Qinling (MY) [45,46]. The fields for HIMU and EM I (enriched mantle I) mantle components are from [69].

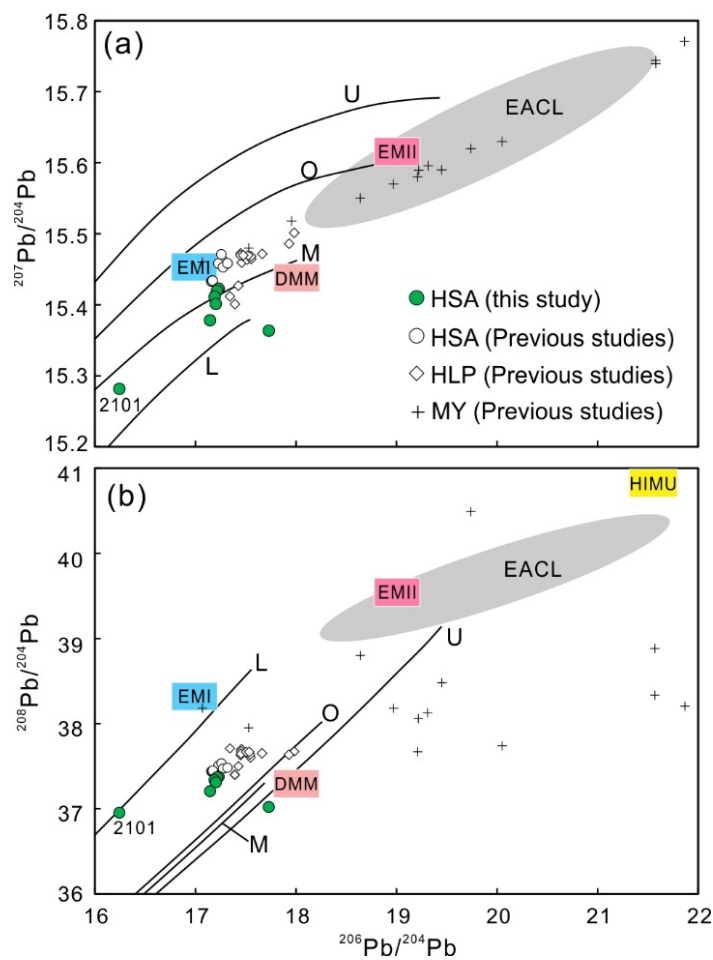


**Figure 6.** Diagrams of initial  $^{207}\text{Pb}/^{204}\text{Pb}$  (a) and initial  $^{208}\text{Pb}/^{204}\text{Pb}$  (b) vs.  $^{206}\text{Pb}/^{204}\text{Pb}$  values for samples of HSA carbonatite. These are compared to initial Pb isotope data reported for those

carbonatites from Lesser Qinling (HSA and HLP) [30,31] and South Qinling (MY) [45,46]. These Pb isotopic features for EACL carbonatites are from [20]. The fields for HIMU, EM I, EM II, and DMM (depleted MORB mantle) mantle components are from [69]. The trends for U (upper crust), O (orogenic belt), M (mantle) and L (lower crust) are from [70].

The initial Pb isotope values for samples of HSA carbonatite define the following ranges:  $^{206}\text{Pb}/^{204}\text{Pb}$  (16.24–17.73),  $^{207}\text{Pb}/^{204}\text{Pb}$  (15.28–15.42), and  $^{208}\text{Pb}/^{204}\text{Pb}$  (36.95–37.38), respectively. In general, the five samples investigated here show similar Pb isotope values compared to those previously reported for HSA and HLP carbonatites from Lesser Qinling [30,31]. Moreover, they have similar  $^{206}\text{Pb}/^{204}\text{Pb}$  and  $^{207}\text{Pb}/^{204}\text{Pb}$  but lower  $^{208}\text{Pb}/^{204}\text{Pb}$  ratios compared to those for the EM I mantle component (Figure 6). Of note, sample HSA2106 is characterized by relatively low initial Pb isotope ratios (Table S4, Figure 7) and associated with a lighter  $\delta^{18}\text{O}_{\text{SMOW}}$  composition (Figure 5).

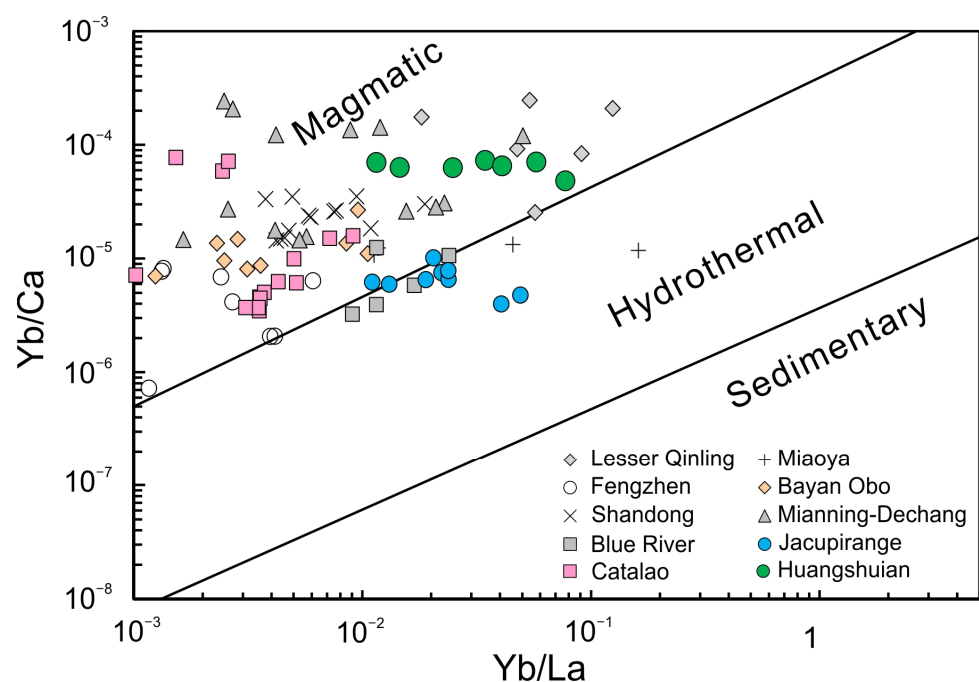


**Figure 7.** Yb/La vs. Yb/Ca diagram for HSA carbonatites [71]. These are compared to those carbonatites from Lesser Qinling reported previously by [31,33]; Miaoya [46], Fengzhen [47], Bayan Obo [72], Shandong [73], Mianning-Dechang [48], Blue River, Canada [66], Jacupirange, Brazil [74], and Catalao, Brazil [75].

## 5. Discussion

### 5.1. Petrogenesis of the HSA Carbonatites

The stable carbon and oxygen isotopic values for these Lesser Qinling carbonatites plot mainly within the primary igneous carbonatite field (Figure 4), which is indicative of their pristine nature and derivation from mantle sources. Moreover, due to their low viscosity and high contents of both Sr and Nd, the feasibility of contamination of carbonatite magma is negligible [1]. Compared to the primitive mantle, HSA carbonatites exhibit enrichment in Sr, Ba, U, and Pb and depletion in HFSEs such as Nb, Ta, Zr, Hf and Ti. They also display higher total REE abundances without evident chondrite-normalized, negative Ce and Eu anomalies. They are characterized by negatively sloped chondrite-normalized REE patterns with enrichment of LREE and more pronounced fractionation between LREE and HREE compared to the average calcic carbonatite. Overall, these geochemical features are generally consistent with the characteristics of typical carbonatite worldwide. HSA carbonatites plot within the magmatic field in the Yb/La vs. Yb/Ca diagram (Figure 7).

The exact petrogenetic origin of carbonatites is still uncertain and has been attributed to three principal hypotheses: (1) low-degree, direct partial melting of a carbonate-bearing mantle [76–80]; (2) extensive fractional crystallization of a carbonated silicate magma [81–84]; and (3) liquid immiscibility between silicate and carbonate melts [81,82,85–90].

The Lesser Qinling carbonatites have abundant K-feldspar, quartz, and sulfate minerals, and are closely associated and co-crystallized with mafic minerals that suggest a common magmatic origin (Figure 2) [32,91]; this petrographic mineral assemblage is not common in typical carbonatite. HSA carbonatites record high CaO and low MgO and alkali contents ( $\text{Na}_2\text{O} + \text{K}_2\text{O}$ ), which contrasts with primary carbonatite melt [87,92,93]. Hence, it is difficult to interpret the combined geochemical characteristics of the HSA carbonatites, as well as those from HYC and Bayan Obo [29]. For example, experimental results indicate that carbonatites formed by immiscibility are typically poor in alkali and abundant in silicate [93]. However, the HSA carbonatites contain much higher silicate contents, and are therefore not consistent with these experimental findings. Furthermore, elements such as Mo and W tend to preferentially enter the silicate phase during the liquid immiscibility process between carbonatite and silicate, leading to a lack of potential Mo mineralization associated with carbonatite [32]. Additionally, typical primary igneous carbonatites originating from metasomatized upper mantle source regions, such as the Spitskop carbonates in South Africa [92], are commonly associated with mafic silicate rocks and contain some specific, high-temperature/pressure minerals derived solely from the mantle, such as Cr-rich minerals and diamonds [22]. The HAS carbonatites lack such specific, mantle-derived minerals and contemporaneous related silicic rocks. Therefore, given these features, liquid immiscibility most likely cannot account for the formation of the HAS carbonatites.

Melting experiments conducted on carbonated peridotite produced low-degree partial melts (<1%) that contained relatively high MgO and alkali contents but very low  $\text{SiO}_2$  abundances in equilibrium with mantle peridotite [94,95]. This carbonatite melt is converted from magnesium to calcium by segregated crystallization and  $\text{CO}_2$  release [87,96]. The crystallization differentiation of carbonate, oxides, apatite, olivine, clinopyroxene, and other accessory minerals was interpreted to be critical in transforming primary Mg-rich carbonatite to Ca-rich carbonatite and significantly higher Si and Mo abundances in the Lesser Qinling carbonatitic magmas [17,29,32]. Carbonate minerals commonly present within carbonatites do not readily host incompatible elements such as Mo, REE, Sr, and Ba [3], which are enriched in residual melt. HAS carbonatites are characterized by extremely high Mo, Sr, and Ba contents, which indicates that these carbonatites do not represent the original magma, but likely represent residual melt fractions present in the late stages of carbonatite magma differentiation [17]. Moreover, the differentiated magnesiocarbonatite melt is characterized by low viscosity and is therefore capable of rapid ascent. When the pressure is <2 GPa, the melt composition changes by reacting with the surrounding rock at mantle depth, leading to an increase in CaO/MgO value and forming a calcite-rich composition. Wei [42] suggested that the calcite carbonatites from Caotan, which are also located within Lesser Qinling, are the product of metasomatic interaction between primary dolomitic melts and felsic wall rocks.

The carbonatite magmas resulting from low-degree partial melting of carbonated mantle peridotites and subsequent liquid immiscibility are usually enriched with LREE relative to HREE [97,98]. However, the HAS carbonatites contain higher HREE contents compared to typical carbonatites. The HREE enrichment of the Lesser Qinling carbonatites results in the uncommonly observed flat chondrite normalized REE pattern, and is believed to be the result of a combination of factors. Smith [28] proposed an HREE-enrichment model in which magmatic, HREE-enriched calcite with a relatively flat REE pattern provided a baseline source of secondary REE mineralization. Late-stage alteration with non-LREE-selective ligands may play an important role in forming HREE-enriched carbonatites [28]. Moreover, fractional crystallization of calcite assisted by high Si and alkaline activities will most likely yield primary HREE enrichment in the residual melts [99–101]. Sulfate

complexation may be a preferential ligand for the transport of REE, while the lack of free F-greatly reduces the precipitation of LREE [28,33,101].

In summary, it is hypothesized that HSA carbonatites most likely represent residual melts formed at the late stage of melt differentiation of the original carbonatite magma.

### 5.2. Source of the Carbonatite and Deep Tectonic Processes

Most young (<200 Ma) carbonatites worldwide show variable Sr, Nd, and Pb isotopic compositions overlapping with those for oceanic island basalts (OIBs), which indicate derivation from a heterogeneous mantle source involving HIMU, EMI, and FOZO mantle components [1,15,17,20]. The EMI-type mantle end members are characterized by high  $^{87}\text{Sr}/^{86}\text{Sr}$ , low  $^{143}\text{Nd}/^{144}\text{Nd}$ , and moderate Pb isotope values [26], which may include the component of recycled subducted oceanic crust/continental lower crust, or old continental lithospheric mantle. The HIMU-type mantle component (characterized by a high  $^{238}\text{U}/^{204}\text{Pb}$  ratio) [25] is associated with recirculating ancient altered oceanic crust, or old carbonate-metasomatic lithospheric mantle [102–104]. The FOZO-type mantle component, with depleted Sr and Nd but fairly radiogenic Pb isotope values, is a mixed end member representing the average components of the lower mantle [26].

All the stable C and O isotopic values reported for the Lesser Qinling carbonatites indicate their pristine nature and origin from the mantle. The oxygen isotopes of quartz in HLP carbonatites ( $\delta^{18}\text{O}_{\text{H}_2\text{O}} = 8.1\text{--}10.2$ ) [32] and quartz in HSA Mo deposits ( $\delta^{18}\text{O}_{\text{H}_2\text{O}} = 7.4\text{--}10.1$ ) [55] indicate a magmatic origin, while sulfur isotopes exhibit characteristics consistent with sulfur from the mantle. The Sr-Nd-Pb isotopic diagrams in Figures 6 and 8 display data for the Lesser Qinling (HAS and HLP) carbonatites and are compared to those for carbonatites worldwide (e.g., East African, North America, Brazil, Bayan Obo, Miaoya, Fengzhen and Shandong from China). The Sr, Nd, and Pb isotopic compositions for the HSA carbonatites are slightly more radiogenic compared to those for the HLP carbonatites. However, isotope compositions from both complexes show characteristics similar to that of EMI-type mantle, far removed from the depleted DMM end member (Figure 5), indicating significant involvement of an enriched end member, possibly such as continental crust. The Pb isotopic characteristics of these carbonatites are significantly distinct compared to those from the Precambrian rocks in the North China Block, but similar to those of basement rocks in the South Qinling [30]. The ratios of  $^{206}\text{Pb}/^{204}\text{Pb}$  and  $^{208}\text{Pb}/^{204}\text{Pb}$  for the Lesser Qinling carbonatites differ from those of carbonatites from the East African Rift, but plot between the average Pb isotope evolution curves for orogenic terranes and mantle (Figure 6a). In Figure 6b, the carbonatites mainly plot between the Pb isotope evolution curves for the lower crust and orogenic terranes [70], which may reflect the orogenic event associated with the subduction of the Mianlue Ocean beneath the South Qinling orogenic belt. Overall, the Lesser Qinling carbonatites display enriched radiogenic Sr-Nd-Pb isotopic compositions (negative  $\epsilon\text{Nd}$  values and high, relatively constant initial  $^{87}\text{Sr}/^{86}\text{Sr}$  and Pb isotopic ratios) compared to typical carbonatites globally, with the exception of the Shandong carbonatites (Figure 8). The latter carbonatites display isotopic signatures that represent a mixture between an EMI-like mantle source and the basement rocks (Taihua and Xiong'er Groups). Here, the Sr-Nd-Pb isotopic compositions of Lesser Qinling carbonatites are best explained as melts derived from an EMI-like mantle source that have subsequently experienced minor contamination of Xiong'er and Taihua basement (Figure 8). Alternatively, the Lesser Qinling carbonatites may have originated as low-degree partial melts from a volumetrically small (distinct), metasomatized, and isotopically heterogeneous section of the upper mantle within this region of the North China Block.



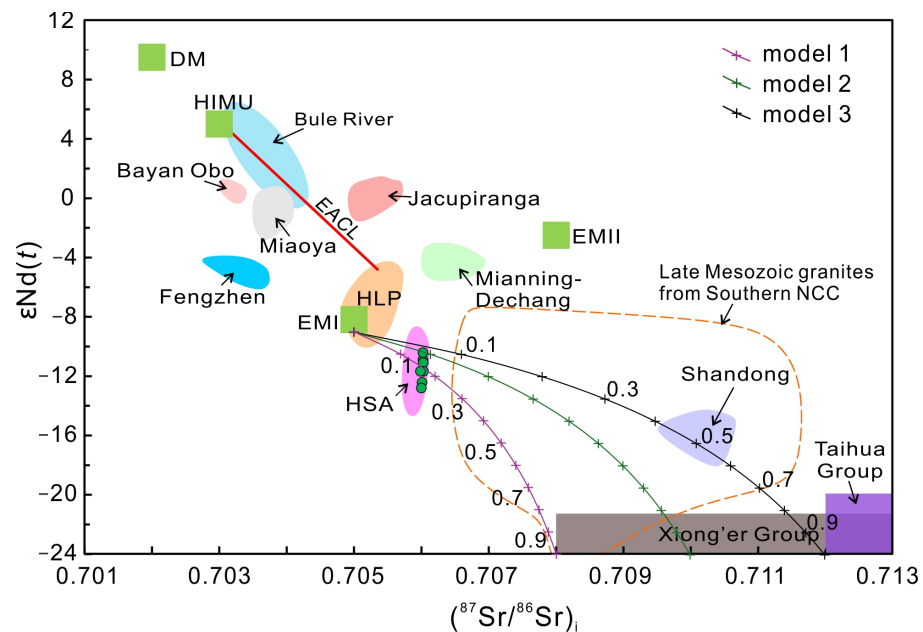


**Figure 8.** Diagrams of initial  $^{87}\text{Sr}/^{86}\text{Sr}$  vs.  $\epsilon_{\text{Nd}}(t)$  values for samples of those carbonatites from China [30,31,45–48,72,73,105]. These are compared to initial Sr and Nd isotope data reported for EACL carbonatites [20], Blue River carbonatites from Canada [66], and Jacupiranga carbonatites from Brazil [65]. The fields for Late Mesozoic granites, Taihua Group, and Xiong'er Group are from [33,106]. The fields for DM, HIMU, EM I and EM II mantle components are from [69]. Binary mixing model curves between the assumed EM I and Xiong'er Group. The  $\epsilon_{\text{Nd}}(t)$  is assumed to be  $-9$  in the EM I and  $-24$  in the Xiong'er Group in the models. The  $(^{87}\text{Sr}/^{86}\text{Sr})_i$  of 0.705 is adopted for EM I in 3 models. The  $(^{87}\text{Sr}/^{86}\text{Sr})_i$  of the Xiong'er Group is taken to be 0.708, 0.709, and 0.710 in models 1, 2, and 3, respectively. A mixture of 10% Xiong'er Group and 90% EM I is represented by 0.1.

Previous studies have proposed that most of the world's carbonatites derive from carbonated lithospheric mantle, and are triggered by either asthenospheric upwelling or plume activity [1,22]. However, this tectonic model is less plausible for the generation of carbonatite magma within orogenic belts. Recently, several studies have focused on the genesis of carbonatite magmas within an orogenic regime and how these relate to the subduction process [3,30,47,48,107–110]. Xu [110] proposed that the carbonatite complexes located within orogenic belts may result from the low-degree melting of subcontinental lithospheric mantle metasomatized by melts/fluids derived from the subduction of terrigenous carbon-rich sediments. The trace element-enriched nature of Chinese carbonatites found within orogenic belts indicates a contribution of recycled crustal material to their mantle source through subduction fluid metasomatism (Figure 9). The subduction of surface carbon into the deep mantle not only provides oxygen-rich components for a more reduced mantle source region, but also facilitates REE enrichment in parent carbonatite magma and formation of REE deposits [3,111–113]. Recent investigations of the B and Ca isotope compositions for carbonatite complexes worldwide are consistent with the hypothesis that the source of the younger ( $<300$  Ma) carbonatites records the input of recycled crustal carbonates [3,14,114,115]. The low-Mg isotopic compositions ( $\delta^{26}\text{Mg} = -1.89\sim-1.07\%$ ) [3] of the HYC carbonatites overlap those of Mesozoic marine dolomites ( $<-1.0\%$ ) [116], which also suggests a recycled sedimentary contribution in their mantle sources [3]. A recent study of an Afghanistan carbonatite occurrence proposed that magmas can efficiently recycle sedimentary carbon from subducting slabs into the overlying lithospheric mantle [117].

During the Early Triassic, the oceanic crust of the Mianlue Ocean subducted beneath the South Qinling Orogen Belt, resulting in a significant influx of carbonate sediments into the mantle peridotite [3,29,45]. The subcontinental lithospheric mantle could be

metasomatically reworked by carbonate-rich melts derived from EMI-type recycled crust components [30]. Subsequently, in the Middle Triassic, the collision between the QOB and the North China Block led to the formation of a series of NW- and NWW-trending fault zones [118–122]. In the Late Triassic period following ocean closure, post-collisional extension induced upwelling of asthenosphere material. This led to low-degree partial melting of carbonated mantle peridotite and subsequent formation of carbonatite magmas. These magmas ascended along trans-lithospheric faults at craton edges resulting in the emplacement of Lesser Qingling carbonatites including HSA, HLP, and HYC [33,36,37].

Overall, the combined Sr-Nd-Pb isotopic compositions for the HSA carbonatites support the hypotheses that the Lesser Qinling carbonatites originate from a heterogeneous upper mantle source involving an EMI-like mantle component and minor assimilation of the basement rocks. The Lesser Qinling carbonatite magmas were derived from the direct melting of the carbonated subcontinental lithospheric mantle, which metasomatized the early subduction of the Mianlue oceanic crust during the incipient stages of the regional orogenic regime.

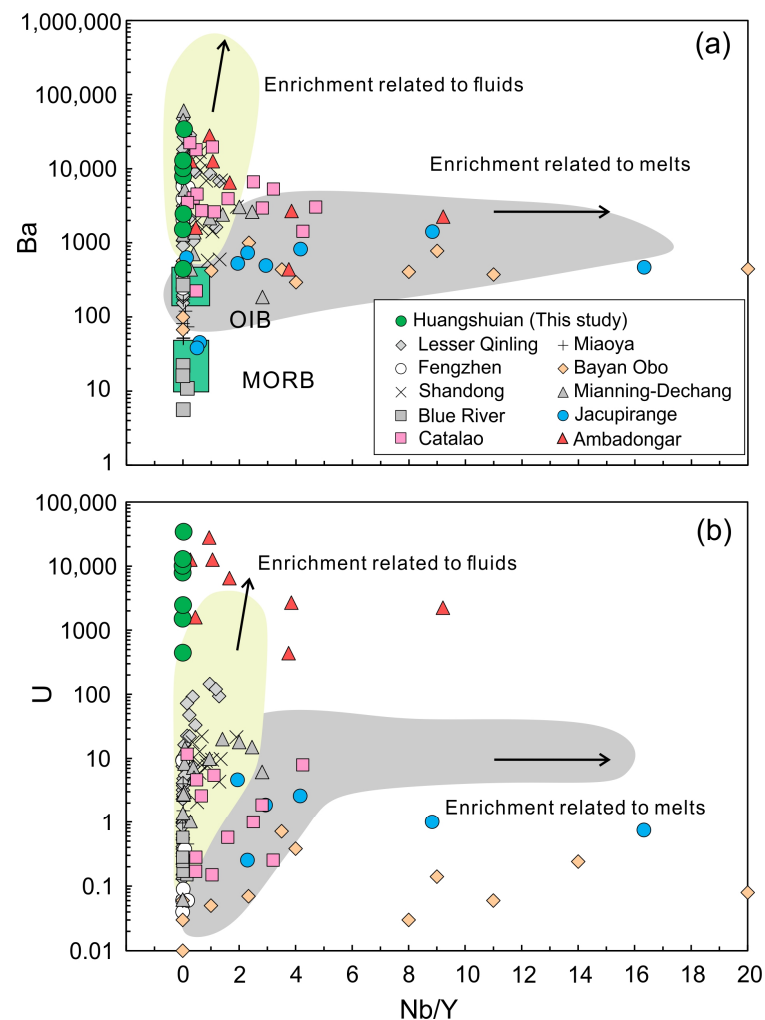


**Figure 9.** Diagrams of Ba (ppm) vs. Nb/Y (a) and U (ppm) vs. Nb/Y (b) for HSA carbonatite and other carbonatites worldwide (references after Figure 7 and Ambadongar, India [123]).

## 6. Conclusions

- (1) The Huangshuian carbonatites in Lesser Qinling Orogen display elevated CaO and low MgO and alkali contents, as well as significant enrichments of Pb, Mo, and HREE, compared to typical carbonatites. The stable C and O isotope compositions suggest

their pristine nature and derivation from mantle source(s). It is postulated that Huangshuian carbonatites represent residual melts of late-stage magmatic differentiation from the parental carbonatite magma.

- (2) The combined Sr-Nd-Pb isotopic compositions for the carbonatites support the hypothesis that the Lesser Qinling carbonatites were derived from a heterogeneous upper mantle source involving an EMI-like mantle component and minor assimilation of the basement rocks.
- (3) We propose that the Lesser Qinling carbonatite magmas were derived directly from the melting of the carbonate-bearing subcontinental lithospheric mantle metasomatized by the subduction of the Mianlue Ocean during the early phase of the regional orogenic tectonism during the Early Triassic.

**Supplementary Materials:** The following supporting information can be downloaded at <https://www.mdpi.com/article/10.3390/min14090953/s1>. Table S1: Major and trace elements compositions of the Huangshuian carbonatites in Lesser Qinling; Table S2: C–O isotopic compositions of the Huangshuian carbonatites in Lesser Qinling; Table S3: Sr–Nd isotopic compositions of the Huangshuian carbonatites in Lesser Qinling; Table S4: Pb isotopic compositions of the Huangshuian carbonatites in Lesser Qinling.

**Author Contributions:** Methodology, A.S., S.S. and Y.D.; formal analysis, H.Z. and S.S.; investigation, H.Z.; data curation, S.S.; writing—original draft, H.Z.; writing—review and editing, H.Z., A.S., X.C. and Y.D.; visualization, H.Z.; supervision, A.S.; funding acquisition, X.C. and Y.D. All authors have read and agreed to the published version of the manuscript.

**Funding:** This study was financially supported by Projects of Shengli Oilfield Sinopec (YKY2401, YKB2312).

**Data Availability Statement:** All data generated or analyses are included within this study and its Supplementary Materials.

**Acknowledgments:** We thank three reviewers for their constructive comments and detailed suggestions, which greatly improved the manuscript. We are grateful to Loretta Corcoran and Corinne Kuebler for their assistance with sample preparation, processing, and analyses within the MITERAC clean room laboratories.

**Conflicts of Interest:** Hao Zhao, Xiaopeng Cao and Yushan Du are employees of Shengli Oilfield Sinopec. The authors declare no conflicts of interest.

## References

1. Bell, K.; Simonetti, A. Source of parental melts to carbonatites—critical isotopic constraints. *Mineral. Petrol.* **2010**, *98*, 77–89. [[CrossRef](#)]
2. Woolley, A.R.; Kjarsgaard, B.A. Carbonatite occurrences of the world: Map and database; geological survey of Canada. *Open File* **2008**, 5796. [[CrossRef](#)]
3. Song, W.L.; Xu, C.; Smith, M.P.; Kynicky, J.; Huang, K.J.; Wei, C.W.; Zhou, L.; Shu, Q.H. Origin of unusual HREE-Mo-rich carbonatites in the Qinling orogen, China. *Sci. Rep.* **2016**, *6*, 37377. [[CrossRef](#)] [[PubMed](#)]
4. Woolley, A.R. Carbonatites: Nomenclature, average chemical compositions, and element distribution. In *Carbonatites: Genesis and Evolution*; Unwin Hyman: London, UK, 1989; pp. 1–13.
5. Treiman, A.H.; Schedl, A. Properties of Carbonatite Magma and Processes in Carbonatite Magma Chambers. *J. Geol.* **1983**, *91*, 437–447. [[CrossRef](#)]
6. Krafft, M.; Keller, J. Temperature Measurements in Carbonatite Lava Lakes and Flows from Oldoinyo Lengai, Tanzania. *Science* **1989**, *245*, 168–170. [[CrossRef](#)]
7. Dawson, J.B.; Pinkerton, H.; Norton, G.E.; Pyle, D.M. Physicochemical properties of alkali carbonatite lavas; data from the 1988 eruption of Oldoinyo Lengai, Tanzania. *Geology* **1990**, *18*, 260–263. [[CrossRef](#)]
8. Jones, A.P.; Genge, M.; Carmody, L. Carbonate Melts and Carbonatites. *Rev. Mineral. Geochem.* **2013**, *75*, 289–322. [[CrossRef](#)]
9. Bell, K.; Blenkinsop, J. Neodymium and strontium isotope geochemistry of carbonatites. In *Carbonatites—Genesis and Evolution*; Bell, K., Ed.; Unwin Hyman: London, UK, 1989; pp. 278–300.
10. Bell, K.; Blenkinsop, J.; Cole, T.J.S.; Menagh, D.P. Evidence from Sr isotopes for long-lived heterogeneities in the upper mantle. *Nature* **1982**, *298*, 251–253. [[CrossRef](#)]
11. Bell, K.; Blenkinsop, J. Nd and Sr isotopic compositions of East African carbonatites; implications for mantle heterogeneity. *Geology* **1987**, *15*, 99–102. [[CrossRef](#)]

12. Tilton, G.R.; Bell, K. Sr-Nd-Pb isotope relationships in Late Archean carbonatites and alkaline complexes, Applications to the geochemical evolution of Archean mantle. *Geochim. Cosmochim. Acta* **1994**, *58*, 3145–3154. [[CrossRef](#)]
13. Hoernle, K.; Tilton, G.; Le Bas, M.J.; Duggen, S.; Garbe-Schönberg, D. Geochemistry of oceanic carbonatites compared with continental carbonatites, mantle recycling of oceanic crustal carbonate. *Contrib. Mineral. Petrol.* **2002**, *142*, 520–542. [[CrossRef](#)]
14. Hulett, S.R.W.; Simonetti, A.; Rasbury, E.T.; Hemming, N.G. Recycling of subducted crustal components into carbonatite melts revealed by boron isotopes. *Nat. Geosci.* **2016**, *9*, 904–908. [[CrossRef](#)]
15. Bell, K.; Simonetti, A. Carbonatite Magmatism and Plume Activity, Implications from the Nd, Pb and Sr Isotope Systematics of Oldoinyo Lengai. *J. Petrol.* **1996**, *37*, 1321–1339. [[CrossRef](#)]
16. Doucelance, R.; Hammouda, T.; Moreira, M.; Martins, J.C. Geochemical constraints on depth of origin of oceanic carbonatites: The Cape Verde case. *Geochim. Cosmochim. Acta* **2010**, *74*, 7261–7282. [[CrossRef](#)]
17. Xu, C.; Campbell, I.H.; Allen, C.M.; Huang, Z.L.; Qi, L.; Zhang, H.; Zhang, G.S. Flat rare earth element patterns as an indicator of cumulate processes in the Lesser Qinling carbonatites, China. *Lithos* **2007**, *95*, 267–278. [[CrossRef](#)]
18. Nelson, D.R.; Chivas, A.R.; Chappell, B.W.; McCulloch, M.T. Geochemical and isotopic systematics in carbonatites and implications for the evolution of ocean-island sources. *Geochim. Cosmochim. Acta* **1988**, *52*, 1–17. [[CrossRef](#)]
19. Bailey, D.K. Carbonate magmas. *J. Geol. Soc. Lond.* **1993**, *150*, 637–651. [[CrossRef](#)]
20. Bell, K.; Tilton, G.R. Probing the mantle: The story from carbonatites. *Eos Trans. Am. Geophys. Union* **2002**, *83*, 273–277. [[CrossRef](#)]
21. Bell, K. Carbonatites: Relationships to mantle-plume activity. *Geol. Soc. Am. Spec. Pap.* **2001**, *352*, 267–290.
22. Bell, K.; Rukhlov, A.S. Carbonatites from the Kola Alkaline Province, origin, evolution and source characteristics. In *Phoscorites and Carbonatites from Mantle to Mine, the Key Example of the Kola Alkaline Province*; Mineralogical Society of Great Britain & Ireland: London, UK, 2004; Volume 10, pp. 421–455.
23. Gerlach, D.C.; Cliff, R.A.; Davies, G.R.; Norry, M.; Hodgson, N. Magma sources of the Cape Verdes archipelago, Isotopic and trace element constraints. *Geochim. Cosmochim. Acta* **1988**, *52*, 2979–2992. [[CrossRef](#)]
24. Simonetti, A.; Goldstein, S.L.; Schmidberger, S.S.; Viladkar, S.G. Geochemical and Nd, Pb, and Sr Isotope Data from Deccan Alkaline Complexes—Inferences for Mantle Sources and Plume-Lithosphere Interaction. *J. Petrol.* **1998**, *39*, 1847–1864. [[CrossRef](#)]
25. Hart, S.R. Heterogeneous mantle domains, signatures, genesis and mixing chronologies. *Earth Planet. Sci. Lett.* **1988**, *90*, 273–296. [[CrossRef](#)]
26. Hart, S.R.; Hauri, E.H.; Oschmann, L.A.; Whitehead, J.A. Mantle Plumes and Entrainment, Isotopic Evidence. *Science* **1992**, *256*, 517–520. [[CrossRef](#)]
27. Xu, C.; Kynicky, J.; Chakhmouradian, A.R.; Qi, L.; Song, W.L. A unique Mo deposit associated with carbonatites in the Qinling orogenic belt, central China. *Lithos* **2010**, *118*, 50–60. [[CrossRef](#)]
28. Smith, M.; Kynicky, J.; Xu, C.; Song, W.L.; Spratt, J.; Jeffries, T.; Brtnicky, M.; Kopriva, A.; Cangelosi, D. The origin of secondary heavy rare earth element enrichment in carbonatites: Constraints from the evolution of the Huanglongpu district, China. *Lithos* **2018**, *308*, 65–82. [[CrossRef](#)]
29. Xue, S.; Ling, M.X.; Liu, Y.L.; Kang, Q.Q.; Huang, R.F.; Zhang, Z.K.; Sun, W.D. The formation of the giant Huayangchuan U-Nb deposit associated with carbonatite in the Qingling Orogenic Belt. *Ore Geol. Rev.* **2020**, *122*, 103498. [[CrossRef](#)]
30. Xu, C.; Taylor, R.N.; Kynicky, J.; Chakhmouradian, A.R.; Song, W.L.; Wang, L.J. The origin of enriched mantle beneath North China block, Evidence from young carbonatites. *Lithos* **2011**, *127*, 1–9. [[CrossRef](#)]
31. Hou, Z.Q.; Yang, Z.M.; Li, Z.Q.; Xu, D.X. Geological and geochemical characteristics, metallogenetic mechanism and tectonic setting of carbonatite vein type Mo (Pb) deposits in the East Qinling molybdenum ore belt. *Acta Geol. Sin.* **2009**, *83*, 1968–1984. (In Chinese with English Abstract)
32. Song, W.L.; Xu, C.; Qi, L.; Zhou, L.; Wang, L.J.; Kynicky, J. Genesis of Si-rich carbonatites in Huanglongpu Mo deposit, Lesser Qinling orogen, China and significance for Mo mineralization. *Ore Geol. Rev.* **2015**, *64*, 756–765. [[CrossRef](#)]
33. Bai, T.; Chen, W.; Jiang, S.Y. Evolution of the carbonatite Mo-HREE deposits in the Lesser Qinling Orogen: Insights from in situ geochemical investigation of calcite and sulfate. *Ore Geol. Rev.* **2019**, *113*, 103069. [[CrossRef](#)]
34. Stein, H.J.; Markey, R.J.; Morgan, J.W.; Du, A.; Sun, Y. Highly precise and accurate Re-Os ages for molybdenite from the East Qinling molybdenum belt, Shaanxi Province, China. *Econ. Geol.* **1997**, *92*, 827–835. [[CrossRef](#)]
35. Cao, J.; Ye, H.S.; Li, H.Y.; Li, Z.Y.; Zhang, X.K.; He, W.; Li, C. Geological characteristics and molybdenite Re-Os isotopic dating of Huangshuan carbonatite vein-type Mo(Pb)deposit in Songxian County, Henan Province. *Miner. Depos.* **2014**, *33*, 53–69. (In Chinese with English Abstract)
36. Zhang, W.; Chen, W.T.; Gao, J.F.; Chen, H.K.; Li, J.H. Two episodes of REE mineralization in the Qinling Orogenic Belt, Central China, in-situ U-Th-Pb dating of bastnäsite and monazite. *Miner. Depos.* **2019**, *54*, 1265–1280. [[CrossRef](#)]
37. Chen, H.Y.; Wu, C.; Jiang, H.J.; Gao, C.; Kang, Q.Q.; Yang, C.S.; Wang, D.E.; Lai, C. Genesis of the supergiant Huayangchuan carbonatite-hosted uranium-polymetallic deposit in the Qinling Orogen, Central China. *Gondwana Res.* **2020**, *86*, 250–265.
38. Mao, J.W.; Xie, G.Q.; Bierlein, F.; Qü, W.J.; Du, A.D.; Ye, H.S.; Pirajno, F.; Li, H.M.; Guo, B.J.; Li, Y.F.; et al. Tectonic implications from Re–Os dating of Mesozoic molybdenum deposits in the East Qinling–Dabie orogenic belt. *Geochim. Cosmochim. Acta* **2008**, *72*, 4607–4626. [[CrossRef](#)]
39. Li, N.; Pirajno, F. Early Mesozoic Mo mineralization in the Qinling Orogen, An overview. *Ore Geol. Rev.* **2017**, *81*, 431–450. [[CrossRef](#)]
40. Kynicky, J.; Smith, M.P.; Xu, C. Diversity of Rare Earth Deposits: The Key Example of China. *Elements* **2012**, *8*, 361–367. [[CrossRef](#)]



41. Huang, G.W.; Pan, C.R.; Pan, J.Y.; Zhong, F.J.; Chen, Z.L.; Xia, F.; Yan, J.; Wu, D.H.; Min, Z. REE mineralization age and geodynamic setting of the Huanglongpu deposit in the East Qinling orogen, China: Evidence from mineralogy, U–Pb geochronology, and in-situ Nd isotope. *Ore Geol. Rev.* **2023**, *152*, 105255. [[CrossRef](#)]
42. Wei, C.W.; Xu, C.; Chakhmouradian, A.R.; Brenna, M.; Kynicky, J.; Song, W.L. Carbon–Strontium Isotope Decoupling in Carbonatites from Caotan (Qinling, China): Implications for the Origin of Calcite Carbonatite in Orogenic Settings. *J. Petrol.* **2020**, *61*, ega024. [[CrossRef](#)]
43. Yaxley, G.M.; Brey, G.P. Phase relations of carbonate-bearing eclogite assemblages from 2.5 to 5.5 GPa: Implications for petrogenesis of carbonatites. *Contrib. Mineral. Petrol.* **2004**, *146*, 606–619. [[CrossRef](#)]
44. Thomson, A.R.; Walter, M.J.; Kohn, S.C.; Brooker, R.A. Slab melting as a barrier to deep carbon subduction. *Nature* **2016**, *529*, 76–79. [[CrossRef](#)] [[PubMed](#)]
45. Xu, C.; Chakhmouradian, A.R.; Taylor, R.N.; Kynicky, J.; Li, W.B.; Song, W.L.; Fletcher, I.R. Origin of carbonatites in the South Qinling orogen, Implications for crustal recycling and timing of collision between the South and North China Blocks. *Geochim. Cosmochim. Acta* **2014**, *143*, 189–206. [[CrossRef](#)]
46. Çimen, O.; Kuebler, C.; Monaco, B.; Simonetti, S.S.; Corcoran, L.; Chen, W.; Simonetti, A. Boron, carbon, oxygen and radiogenic isotope investigation of carbonatite from the Miaoya complex, central China, Evidences for late-stage REE hydrothermal event and mantle source heterogeneity. *Lithos* **2018**, *322*, 225–237. [[CrossRef](#)]
47. Xu, C.; Kynický, J.; Song, W.L.; Tao, R.B.; Lü, Z.; Li, Y.X.; Yang, Y.H.; Pohanka, M.; Galiova, M.V.; Zhang, L.F.; et al. Cold deep subduction recorded by remnants of a Paleoproterozoic carbonated slab. *Nat. Commun.* **2018**, *9*, 2790. [[CrossRef](#)]
48. Hou, Z.Q.; Tian, S.H.; Yuan, Z.X.; Xie, Y.L.; Yin, S.P.; Yi, L.S.; Fei, H.C.; Yang, Z.M. The Himalayan collision zone carbonatites in western Sichuan, SW China, Petrogenesis, mantle source and tectonic implication. *Earth Planet. Sci. Lett.* **2006**, *244*, 234–250. [[CrossRef](#)]
49. Zhang, G.W.; Meng, Q.G.; Lai, S.C. Tectonics and structure of Qinling Orogenic Belt. *Sci. China Ser. B* **1995**, *38*, 1379–1394.
50. Kröner, A.; Compston, W.; Zhang, G.W.; Guo, A.L.; Todt, W. Age and tectonic setting of Late Archean greenstone-gneiss terrain in Henan Province, China, as revealed by single-grain zircon dating. *Geology* **1988**, *16*, 211–215. [[CrossRef](#)]
51. Peng, P.; Zhai, M.G.; Ernst, R.E.; Guo, J.H.; Liu, F.; Hu, B. A 1.78 Ga large igneous province in the North China craton, The Xiong'er Volcanic Province and the North China dyke swarm. *Lithos* **2008**, *101*, 260–280. [[CrossRef](#)]
52. Zhao, G.C.; He, Y.H.; Sun, M. The Xiong'er volcanic belt at the southern margin of the North China Craton: Petrographic and geochemical evidence for its outboard position in the Paleo-Mesoproterozoic Columbia Supercontinent. *Gondwana Res.* **2009**, *16*, 170–181. [[CrossRef](#)]
53. Zhang, C.L.; Wang, T.; Wang, X.X. Origin and tectonic setting of the Early Mesozoic granitoids in Qinling orogenic belt. *Geol. J. China Univ.* **2008**, *14*, 304–316.
54. Mao, J.W.; Xie, G.Q.; Pirajno, F.; Ye, H.S.; Wang, Y.B.; Li, Y.F.; Xiang, J.F.; Zhao, H.J. Late Jurassic-Early Cretaceous granitoid magmatism in Eastern Qinling, central-eastern China: SHRIMP zircon U-Pb ages and tectonic implications. *Aust. J. Earth Sci.* **2010**, *57*, 51–78. [[CrossRef](#)]
55. Cao, J.; Ye, H.S.; Chen, X.D.; He, W.; Wang, P. Geochemistry, Zircon U–Pb Age, and Lu–Hf Isotope of the Granite Porphyry in Leimengou Mo Deposit in the East Qinling Molybdenum Ore Belt, China. *Minerals* **2018**, *8*, 293. [[CrossRef](#)]
56. Jenner, G.A.; Longerich, H.P.; Jackson, S.E.; Fryer, B.J. ICP-MS—A powerful tool for high-precision trace-element analysis in Earth sciences: Evidence from analysis of selected U.S.G.S. reference samples. *Chem. Geol.* **1990**, *83*, 133–148. [[CrossRef](#)]
57. McCrea, J.M. On the Isotopic Chemistry of Carbonates and a Paleotemperature Scale. *J. Chem. Phys.* **1950**, *18*, 849–857. [[CrossRef](#)]
58. Balboni, E.; Jones, N.; Spano, T.; Simonetti, A.; Burns, P.C. Chemical and Sr isotopic characterization of North America uranium ores, Nuclear forensic applications. *Appl. Geochem.* **2016**, *74*, 24–32. [[CrossRef](#)]
59. Tanaka, T.; Togashi, S.; Kamioka, H.; Amakawa, H.; Kagami, H.; Hamamoto, T.; Yuhara, M.; Orihashi, Y.; Yoneda, S.; Shimizu, H.; et al. JNdi-1, a neodymium isotopic reference in consistency with LaJolla neodymium. *Chem. Geol.* **2000**, *168*, 279–281. [[CrossRef](#)]
60. Simonetti, A.; Gariépy, C.; Banic, C.M.; Tanabe, R.; Wong, H.K. Pb isotopic investigation of aircraft-sampled emissions from the Horne smelter (Rouyn, Québec), Implications for atmospheric pollution in northeastern North America. *Geochim. Cosmochim. Acta* **2004**, *68*, 3285–3294. [[CrossRef](#)]
61. Manhès, G.; Minster, J.F.; Allègre, C.J. Comparative uranium-thorium-lead and rubidium-strontium study of the Saint Séverin amphoterite, consequences for early solar system chronology. *Earth Planet. Sci. Lett.* **1978**, *39*, 14–24. [[CrossRef](#)]
62. Baker, J.; Peate, D.; Waight, T.; Meyzen, C. Pb isotopic analysis of standards and samples using a 207Pb–204Pb double spike and thallium to correct for mass bias with a double-focusing MC-ICP-MS. *Chem. Geol.* **2004**, *211*, 275–303. [[CrossRef](#)]
63. Kjarsgaard, B.A. The genesis of carbonatites by immiscibility. In *Carbonatites: Genesis and Evolution*; Unwin Hyman: London, UK, 1989; pp. 388–404.
64. Sun, S.S.; McDonough, W.F. Chemical and isotopic systematics of oceanic basalts, implications for mantle composition and processes. *Geol. Soc. Spec. Publ.* **1989**, *42*, 313–345. [[CrossRef](#)]
65. Huang, Y.M.; Hawkesworth, C.J.; van Calsteren, P.; McDermott, F. Geochemical characteristics and origin of the Jacupiranga carbonatites, Brazil. *Chem. Geol.* **1995**, *119*, 79–99. [[CrossRef](#)]
66. Çimen, O.; Kuebler, C.; Simonetti, S.S.; Corcoran, L.; Mitchell, R.; Simonetti, A. Combined boron, radiogenic (Nd, Pb, Sr), stable (C, O) isotopic and geochemical investigations of carbonatites from the Blue River Region, British Columbia (Canada), Implications for mantle sources and recycling of crustal carbon. *Chem. Geol.* **2019**, *529*, 119240. [[CrossRef](#)]

67. Keller, J.; Hoefs, J. Stable Isotope Characteristics of Recent Natrocarbonatites from Oldoinyo Lengai. In *Carbonatite Volcanism*; Springer: Berlin/Heidelberg, Germany, 1995; pp. 113–123.
68. Demény, A.; Ahijado, A.; Casillas, R.; Vennemann, T.W. Crustal contamination and fluid/rock interaction in the carbonatites of Fuerteventura (Canary Islands, Spain), a C, O, H isotope study. *Lithos* **1998**, *44*, 101–115. [[CrossRef](#)]
69. Zindler, A.; Hart, S.R. Chemical geodynamics. *Annu. Rev. Earth Planet. Sci.* **1986**, *14*, 493–571. [[CrossRef](#)]
70. Zartman, R.E.; Doe, B.R. Plumbotectonics—The model. *Tectonophysics* **1981**, *75*, 135–162. [[CrossRef](#)]
71. Möller, P.; Parekh, P.P.; Schneider, H.J. The application of Tb/Ca-Tb/La abundance ratios to problems of fluor spar genesis. *Miner. Depos.* **1976**, *11*, 111–116. [[CrossRef](#)]
72. Kuebler, C.; Simonetti, A.; Chen, W.; Simonetti, S.S. Boron isotopic investigation of the Bayan Obo carbonatite complex, Insights into the source of mantle carbon and hydrothermal alteration. *Chem. Geol.* **2020**, *557*, 119859. [[CrossRef](#)]
73. Ying, Y.F.; Zhou, X.H.; Zhang, H.F. Geochemical and isotopic investigation of the Laiwu-Zibo carbonatites from western Shandong Province, China, and implications for their petrogenesis and enriched mantle source. *Lithos* **2004**, *75*, 413–426. [[CrossRef](#)]
74. Chmyz, L.; Arnaud, N.; Biondi, J.C.; Azzone, R.G.; Bosch, D.; Ruberti, E. Ar-Ar ages, Sr-Nd isotope geochemistry, and implications for the origin of the silicate rocks of the Jacupiranga ultramafic-alkaline complex (Brazil). *J. S. Am. Earth Sci.* **2017**, *77*, 286–309. [[CrossRef](#)]
75. Guarino, V.; Wu, F.; Melluso, L.; de Barros Gomes, C.; Tassinari, C.C.G.; Ruberti, E.; Brilli, M. U–Pb ages, geochemistry, C–O–Nd–Sr–Hf isotopes and petrogenesis of the Catalão II carbonatitic complex (Alto Paranaíba Igneous Province, Brazil): Implications for regional-scale heterogeneities in the Brazilian carbonatite associations. *Int. J. Earth Sci.* **2017**, *106*, 1963–1989. [[CrossRef](#)]
76. Wyllie, P.J.; Huang, W. Influence of mantle CO<sub>2</sub> in the generation of carbonatites and kimberlites. *Nature* **1975**, *257*, 297–299. [[CrossRef](#)]
77. Green, D.H.; Wallace, M.E. Mantle metasomatism by ephemeral carbonatite melts. *Nature* **1988**, *336*, 459–462. [[CrossRef](#)]
78. Moore, K.R.; Wood, B.J. The Transition from Carbonate to Silicate Melts in the CaO–MgO–SiO<sub>2</sub>–CO<sub>2</sub> System. *J. Petrol.* **1998**, *39*, 1943–1951. [[CrossRef](#)]
79. Wyllie, P.J.; Lee, W.J. Model System Controls on Conditions for Formation of Magnesiocarbonatite and Calcicarbonatite Magmas from the Mantle. *J. Petrol.* **1998**, *39*, 1885–1893. [[CrossRef](#)]
80. Grassi, D.; Schmidt, M.W. Melting of carbonated pelites at 8–13 GPa, generating K-rich carbonatites for mantle metasomatism. *Contrib. Mineral. Petrol.* **2011**, *162*, 169–191. [[CrossRef](#)]
81. Lee, W.J.; Wyllie, P.J. Experimental Data Bearing on Liquid Immiscibility, Crystal Fractionation, and the Origin of Calcicarbonatites and Natrocarbonatites. *Int. Geol. Rev.* **1994**, *36*, 797–819. [[CrossRef](#)]
82. Lee, W.J.; Wyllie, P.J. Processes of Crustal Carbonatite Formation by Liquid Immiscibility and Differentiation, Elucidated by Model Systems. *J. Petrol.* **1998**, *39*, 2005–2013. [[CrossRef](#)]
83. Veksler, I.V.; Petibon, C.; Jenner, G.A.; Dorfman, A.M.; Dingwell, D.B. Trace Element Partitioning in Immiscible Silicate–Carbonate Liquid Systems: An Initial Experimental Study Using a Centrifuge Autoclave. *J. Petrol.* **1998**, *39*, 2095–2104. [[CrossRef](#)]
84. Doroshkevich, A.G.; Veksler, I.V.; Klemd, R.; Khromova, E.A.; Izbrodin, I.A. Trace-element composition of minerals and rocks in the Belaya Zima carbonatite complex (Russia): Implications for the mechanisms of magma evolution and carbonatite formation. *Lithos* **2017**, *284–285*, 91–108. [[CrossRef](#)]
85. Lee, W.J.; Wyllie, P.J. Liquid immiscibility between nephelinite and carbonatite from 1.0 to 2.5 GPa compared with mantle melt compositions. *Contrib. Mineral. Petrol.* **1997**, *127*, 1–16. [[CrossRef](#)]
86. Veksler, I.V.; Nielsen, T.F.D.; Sokolov, S.V. Mineralogy of Crystallized Melt Inclusions from Gardiner and Kovdor Ultramafic Alkaline Complexes, Implications for Carbonatite Genesis. *J. Petrol.* **1998**, *39*, 2015–2031. [[CrossRef](#)]
87. Lee, W.J.; Wyllie, P.J. The system CaO–MgO–SiO<sub>2</sub>–CO<sub>2</sub> at 1 GPa, metasomatic wehrlites, and primary carbonatite magmas. *Contrib. Mineral. Petrol.* **2000**, *138*, 214–228. [[CrossRef](#)]
88. Rosatelli, G.; Wall, F.; Stoppa, F. Calcio-carbonatite melts and metasomatism in the mantle beneath Mt. Vulture (Southern Italy). *Lithos* **2007**, *99*, 229–248. [[CrossRef](#)]
89. Fischer, T.P.; Burnard, P.; Marty, B.; Hilton, D.R.; Füri, E.; Palhol, F.; Sharp, Z.D.; Mangasini, F. Upper-mantle volatile chemistry at Oldoinyo Lengai volcano and the origin of carbonatites. *Nature* **2009**, *459*, 77–80. [[CrossRef](#)] [[PubMed](#)]
90. Potter, N.J.; Kamenetsky, V.S.; Simonetti, A.; Goemann, K. Different types of liquid immiscibility in carbonatite magmas, A case study of the Oldoinyo Lengai 1993 lava and melt inclusions. *Chem. Geol.* **2017**, *455*, 376–384. [[CrossRef](#)]
91. Cangelosi, D.; Smith, M.; Banks, D.; Yardley, B. The role of sulfate-rich fluids in heavy rare earth enrichment at the Dashigou carbonatite deposit, Huanglongpu, China. *Mineral. Mag.* **2020**, *84*, 65–80. [[CrossRef](#)]
92. Harmer, R.E.; Gittins, J. The Case for Primary, Mantle-derived Carbonatite Magma. *J. Petrol.* **1998**, *39*, 1895–1903. [[CrossRef](#)]
93. Brooker, R.A.; Kjarsgaard, B.A. Silicate–carbonate liquid immiscibility and phase relations in the system SiO<sub>2</sub>–Na<sub>2</sub>O–Al<sub>2</sub>O<sub>3</sub>–CaO–CO<sub>2</sub> at 0.1–2.5 GPa with applications to carbonatite genesis. *J. Petrol.* **2011**, *52*, 1281–1305. [[CrossRef](#)]
94. Wallace, M.E.; Green, D.H. An experimental determination of primary carbonatite magma composition. *Nature* **1988**, *335*, 343–346. [[CrossRef](#)]
95. Dalton, J.A.; Presnall, D.C. The Continuum of Primary Carbonatitic–Kimberlitic Melt Compositions in Equilibrium with Lherzolite, Data from the System CaO–MgO–Al<sub>2</sub>O<sub>3</sub>–SiO<sub>2</sub>–CO<sub>2</sub> at 6 GPa. *J. Petrol.* **1998**, *39*, 1953–1964. [[CrossRef](#)]
96. Dasgupta, R.; Hirschmann, M.M.; Stalker, K. Immiscible transition from carbonate-rich to silicate-rich melts in the 3 GPa melting interval of eclogite plus CO<sub>2</sub> and genesis of sili-ca-under-saturated ocean island lavas. *J. Petrol.* **2006**, *47*, 647–671. [[CrossRef](#)]

97. Martin, L.H.J.; Schmidt, M.W.; Mattsson, H.B.; Ulmer, P.; Hametner, K.; Günther, D. Element partitioning between immiscible carbonatite–kamafugite melts with application to the Italian ultrapotassic suite. *Chem. Geol.* **2012**, *320–321*, 96–112. [[CrossRef](#)]
98. Nabyl, Z.; Massuyeau, M.; Gaillard, F.; Tuduri, J.; Iacono-Marziano, G.; Rogerie, G.; Le Trong, E.; Di Carlo, I.; Melleton, J.; Bailly, L. A window in the course of alkaline magma differentiation conducive to immiscible REE-rich carbonatites. *Geochim. Cosmochim. Acta* **2020**, *282*, 297–323. [[CrossRef](#)]
99. Anenburg, M.; Mavrogenes, J.A.; Frigo, C.; Wall, F. Rare earth element mobility in and around carbonatites controlled by sodium, potassium, and silica. *Sci. Adv.* **2020**, *6*, eabb6570. [[CrossRef](#)]
100. Wei, C.W.; Xu, C.; Song, W.L.; Chen, W.; Shi, A.G.; Li, Z.Q.; Fan, C.X. Heavy rare earth element and crustal-derived silicon enrichment in Huayangchuan carbonatites, Qinling orogenic belt. *Lithos* **2023**, *436–437*, 106987. [[CrossRef](#)]
101. Li, F.C.; Zeng, Q.D.; Kang, Q.Q.; Fan, H.R.; Yang, K.F.; She, H.D.; Huang, L.L.; Yu, B.; Wu, J.J. Unusual HREE enrichment and mineralization age in the Jialu deposit from the Qinling Orogen, central China. *Ore Geol. Rev.* **2024**, *166*, 105932. [[CrossRef](#)]
102. Stracke, A.; Hofmann, A.W.; Hart, S.R. FOZO, HIMU, and the rest of the mantle zoo. *Geochem. Geophys. Geosyst.* **2005**, *6*, Q05007. [[CrossRef](#)]
103. Parai, R.; Mukhopadhyay, S.; Lassiter, J.C. New constraints on the HIMU mantle from neon and helium isotopic compositions of basalts from the Cook–Austral Islands. *Earth Planet. Sci. Lett.* **2009**, *277*, 253–261. [[CrossRef](#)]
104. Hanyu, T.; Tatsumi, Y.; Senda, R.; Miyazaki, T.; Chang, Q.; Hirahara, Y.; Takahashi, T.; Kawabata, H.; Suzuki, K.; Kimura, J.; et al. Geochemical characteristics and origin of the HIMU reservoir, A possible mantle plume source in the lower mantle. *Geochem. Geophys. Geosyst.* **2011**, *12*, 1–30. [[CrossRef](#)]
105. Xu, C.; Chakhmouradian, A.R.; Kynický, J.; Li, Y.X.; Song, W.L.; Chen, W. A Paleoproterozoic mantle source modified by subducted sediments under the North China craton. *Geochim. Cosmochim. Acta* **2019**, *245*, 222–239. [[CrossRef](#)]
106. She, H.D.; Fan, H.R.; Yang, K.F.; Li, X.H.; Wang, Z.Y. REEs upgrading by post-carbonatite fluids in the Huangshui’an Mo-REE deposit, eastern Qinling Orogen (central China). *Ore Geol. Rev.* **2022**, *150*, 105177. [[CrossRef](#)]
107. Hou, Z.Q.; Liu, Y.; Tian, S.H.; Yang, Z.M.; Xie, Y.L. Formation of carbonatite-related giant rare-earth-element deposits by the recycling of marine sediments. *Sci. Rep.* **2015**, *5*, 10231. [[CrossRef](#)] [[PubMed](#)]
108. Liu, Y.; Hou, Z.Q. A synthesis of mineralization styles with an integrated genetic model of carbonatite-syenite-hosted REE deposits in the Cenozoic Mianning-Dechang REE metallogenic belt, the eastern Tibetan Plateau, southwestern China. *J. Asian Earth Sci.* **2017**, *137*, 35–79. [[CrossRef](#)]
109. Woodard, J.; Huhma, H. Paleoproterozoic mantle enrichment beneath the Fennoscandian Shield: Isotopic insight from carbonatites and lamprophyres. *Lithos* **2015**, *236*, 311–323. [[CrossRef](#)]
110. Xu, C.; Kynický, J.; Chakhmouradian, A.R.; Li, X.H.; Song, W.L. A case example of the importance of multi-analytical approach in deciphering carbonatite petrogenesis in South Qinling orogen, Miaoya rare-metal deposit, central China. *Lithos* **2015**, *227*, 107–121. [[CrossRef](#)]
111. Ling, M.X.; Liu, Y.L.; Williams, I.S.; Teng, F.Z.; Yang, X.Y.; Ding, X.; Wei, G.J.; Xie, L.H.; Deng, W.F.; Sun, W.D. Formation of the world’s largest REE deposit through protracted fluxing of carbonatite by subduction-derived fluids. *Sci. Rep.* **2013**, *3*, 1776. [[CrossRef](#)]
112. Goodenough, K.M.; Schilling, J.; Jonsson, E.; Kalvig, P.; Charles, N.; Tuduri, J.; Deady, E.A.; Sadeghi, M.; Schiellerup, H.; Müller, A.; et al. Europe’s rare earth element resource potential, An overview of REE metallogenic provinces and their geodynamic setting. *Ore Geol. Rev.* **2016**, *72*, 838–856. [[CrossRef](#)]
113. Yang, K.F.; Fan, H.R.; Pirajno, F.; Li, X.C. The Bayan Obo (China) giant REE accumulation conundrum elucidated by intense magmatic differentiation of carbonatite. *Geology* **2019**, *47*, 1198–1202. [[CrossRef](#)]
114. Amsellem, E.; Moynier, F.; Bertrand, H.; Bouyon, A.; Mata, J.; Tappe, S.; Day, J. Calcium isotopic evidence for the mantle sources of carbonatites. *Sci. Adv.* **2020**, *6*, eaba3269. [[CrossRef](#)]
115. Banerjee, A.; Chakrabarti, R.; Simonetti, A. Temporal evolution of  $\delta^{44}/^{40}\text{Ca}$  and  $^{87}\text{Sr}/^{86}\text{Sr}$  of carbonatites: Implications for crustal recycling through time. *Geochim. Cosmochim. Acta* **2021**, *307*, 168–191. [[CrossRef](#)]
116. Huang, K.J.; Shen, B.; Lang, X.G.; Tang, W.B.; Peng, Y.; Ke, S.; Kaufman, A.J.; Ma, H.R.; Li, F.B. Magnesium isotopic compositions of the Mesoproterozoic dolostones, Implications for Mg isotopic systematics of marine carbonates. *Geochim. Cosmochim. Acta* **2015**, *164*, 333–351. [[CrossRef](#)]
117. Horton, F. Rapid recycling of subducted sedimentary carbon revealed by Afghanistan carbonatite volcano. *Nat. Geosci.* **2021**, *14*, 508–512. [[CrossRef](#)]
118. Meng, Q.R.; Zhang, G.W. Timing of collision of the North and South China blocks: Controversy and reconciliation. *Geology* **1999**, *27*, 123–126. [[CrossRef](#)]
119. Meng, Q.R.; Zhang, G.W. Geologic framework and tectonic evolution of the Qin-ling orogen, central China. *Tectonophysics* **2000**, *323*, 183–196. [[CrossRef](#)]
120. Xu, C.; Song, W.L.; Qi, L.; Wang, L.J. Geochemical characteristic and tectonic setting of ore-bearing carbonatite in Huanglongpu Mo ore field. *Acta Petrol. Sin.* **2009**, *25*, 422–430. (In Chinese with English Abstract)
121. Wu, Y.B.; Zheng, Y.F. Tectonic evolution of a composite collision orogen, An overview on the Qinling–Tongbai–Hong’an–Dabie–Sulu orogenic belt in central China. *Gondwana Res.* **2013**, *23*, 1402–1428. [[CrossRef](#)]

122. Dong, Y.P.; Santosh, M. Tectonic architecture and multiple orogeny of the Qinling Orogenic Belt, Central China. *Gondwana Res.* **2016**, *29*, 1–40. [[CrossRef](#)]
123. Chandra, J.; Paul, D.; Stracke, A.; Chabaux, F.; Granet, M. The Origin of Carbonatites from Amba Dongar within the Deccan Large Igneous Province. *J. Petrol.* **2019**, *60*, 1119–1134. [[CrossRef](#)]

**Disclaimer/Publisher’s Note:** The statements, opinions and data contained in all publications are solely those of the individual author(s) and contributor(s) and not of MDPI and/or the editor(s). MDPI and/or the editor(s) disclaim responsibility for any injury to people or property resulting from any ideas, methods, instructions or products referred to in the content.